Efficient creation of electron vortex beams for high resolution STEM imaging

Reference:

Béché Armand, Juchtmans Roeland, Verbeeck Johan.- Efficient creation of electron vortex beams for high resolution STEM imaging

Ultramicroscopy - ISSN 0304-3991 - (2016), p. 1-8

Full text (Publishers DOI): http://dx.doi.org/doi:10.1016/j.ultramic.2016.05.006

Efficient creation of electron vortex beams for high resolution STEM imaging

A. Béché*[a], R. Juchtmans[a], J. Verbeeck[a]

[a]*EMAT, University of Antwerp, Groenenborgerlaan 171, 2020 Antwerp, Belgium*

Abstract

The recent discovery of electron vortex beams carrying quantised angular momentum in the TEM has led to an active field of research, exploring a variety of potential applications including the possibility of mapping magnetic states at the atomic scale. A prerequisite for this is the availability of atomic sized electron vortex beams at high beam current and mode purity. In this paper we present recent progress showing that by making use of the Aharonov-Bohm effect near the tip of a long single domain ferromagnetic Nickel needle, a very efficient aperture for the production of electron vortex beams can be realised. The aperture transmits more than 99% of all electrons and provides a vortex mode purity of up to 92%. Placing this aperture in the condenser plane of a state of the art Cs corrected microscope allows us to demonstrate atomic resolution HAADF STEM images with spatial resolution better than1 Angstrom, in agreement with theoretical expectations and only slightly inferior to the performance of a non-vortex probe on the same instrument.

Keywords: Electron vortex beam, High Resolution Scanning Transmission Microscopy, Holography.

1. Introduction

Electron vortex beams were only recently experimentally observed in transmission electron microscopy (TEM) after they were earlier predicted on theoretical grounds [1, 2, 3]. Electron vortex beams constitute freely propagating angular momentum eigenstates with a typical circularly symmetric intensity profile, a dark centre and an azimuthally varying phase, much like their optical and electromagnetic counterparts which were developed much earlier [4, 5, 6]. The charged nature of the electron enhances the already interesting properties of optical vortex beams with a quantised magnetic moment in addition to the quantised orbital angular momentum [3, 7]. The very short wavelength of accelerated electrons leads to the possibility of making electron vortex beams with an azimuthal symmetry and radial confinement very similar to atomic orbitals while travelling in free space [8]. A wide range of applications is being investigated, ranging from detecting magnetic information [2], enhancing imaging contrast in TEM [9], providing mechanical torque to nanoparticles [10], determining the handedness of chiral crystals [11], studying Landau states in free space [12], studying transition radiation [13] and many more [9, 14]. Obtaining magnetic information from energy loss magnetic chiral dichroism (EMCD) [15, 2] at the atomic scale is especially attractive. In order to approach this theoretically predicted goal [15, 16, 17]], high purity (majority of the probe in a single orbital angular momentum (OAM) eigenstate), high intensity (majority of the incoming beam is present in the probe) and atomic size vortex beams are required, especially as theoretical predictions forecast that the part of the EELS signal which depends on the local magnetic state will typically constitute less than 10% of the already very faint atomic resolution elemental signal [16].

In recent years, numerous possibilities have been investigated to generate electron vortices, each having different advantages and disadvantages. The now well-known holographic masks [2, 18, 19] provide high

Email address: armand.beche@uantwerpen.be (A. Béché*)

purity electron vortex beams, but the intensity of these pure vortex states is limited to a small fraction (typically 10%) of the total incoming beam, even in the most recent designs [20, 21]. Moreover, the holographic mask method typically results in multiple diffraction-order beams of different vorticity which must be separated, for example by extra selection apertures [22]. When aiming to produce atomic scale vortices, the different diffraction orders are either superimposed [18], or too close to each other to be efficiently separated [19, 20, 21]. An alternative way to create electron vortex beams consists in illuminating an electron transparent film, presenting a spiraling thickness profile, with a plane wave [1]. The interaction of the electron wave with the mean inner potential of the film then creates a spiraling phase shift that can be used to create a vortex beam [23, 24]. This method leads to a single electron probe but obtaining good OAM purity is troublesome as a non-negligible part of the incoming beam is absorbed or scattered by the phase plate itself. Moreover, this type of design is sensitive to contamination. A more exotic technique consists of tuning a Cs-Probe corrector in a particular way such that the phase acquires the required azimuthal character over a limited range of angles which are then selected with a thin annular aperture [25]. The use of the annular aperture makes this technique rather inefficient as most electrons are stopped by the annular aperture and the resulting mode purity is suboptimal due to the crude control of only a limited range of aberration orders. Most importantly, the annular aperture leads to a Bessel-like radial beam profile [26] with significant tails, making atomic resolution impossible. An attractive alternative for making electron vortex beams is to make use of the phase shift induced by the magnetic field around the tip of a long ferromagnetic needle [27]. In the present work, we demonstrate that further optimising this setup leads to high purity vortex beams with very high beam intensity, and state of the art probe size.

2. Sample preparation

A vortex generating aperture is created by mimicking the divergent magnetic field of a magnetic monopole at the end of a long magnetised needle ending in the center of a round aperture. The projected phase shift due to the Aharonov-Bohm effect is then a good approximation of a spiraling phase plate excepting the region of magnetic flux enclosed in the needle. In previous work we fabricated the magnetic needle from a bulk Ni specimen by focused ion beam milling (FIB) leading to a slightly conical shape. This geometry causes deviations from the ideal spiral phase plate as not all the flux reaches the extremities of the needle and leaks out through the sides [27]. To overcome this issue, we now began from a thin film of ferromagnetic material that was shaped into a rod with a rectangular cross section milled from the top side with the FIB. In this way, it is much easier to fulfil the stringent condition of perfect side parallelism.

More precisely, a 60 nm thin nickel layer was sputtered on a 200 nm thick SiN membrane, making use of a FEI Helios Dual-Beam Focused Ion Beam (FIB) microscope. The magnetic layer was then covered with a thick layer of sputtered gold ($\simeq$1 μm) to protect the ferromagnetic film from damage caused by the FIB during the preparation. Two rods of 50x2 μm^2 were extracted from the film using an Omniprobe nanomanipulator. In parallel, a silicon grid presenting in its centre a suspended 100 nm thick SiN membrane of 250x250 μm^2 was coated with sputtered gold to be used as aperture in the TEM. On this support, two 20 μm holes were milled which will serve as two vortex forming apertures with opposite OAM. Making use of the nanomanipulator, the two nickel rods were placed on a line connecting the two aperture holes, making sure that each rod end was in the centre of its own aperture hole. Both rods are then magnetically connected with another 100 μm long nickel rod. This arrangement forms a long and thin magnetic bar with magnetic poles of opposite signs positioned exactly over the centres of the two aperture holes. The interaction of an electron plane wave with these magnetic poles will lead to electron vortices with opposite handedness. In order to fine-tune the magnetic flux in the needles both nickel rods were further thinned while monitoring their phase effect on the electron beam as described in the next section and while keeping the sidewalls as parallel as possible. Doing so, we ended up with the final widths of the rods being respectively 300 and 310 nm (see figure 1). With this design, the electron beam is only blocked by the magnetic rod, which represents less than 1% of the aperture surface. Thus more than 99% of the incoming electron beam intensity will be transferred into the electron probe.

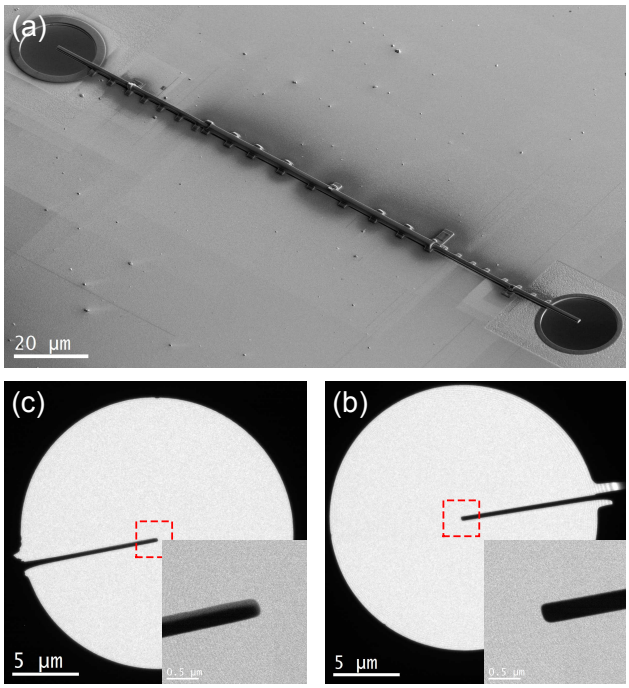

Figure 1: *(a) SEM image of the two rods hanging over the 20 µm apertures holes. The wider rod is also visible in-between the two apertures. (b) TEM image of rod ♯1 with a closer look at the tip in the inset. (c) Same as (b) for rod ♯2.*

3. Obtaining an electron vortex beam

3.1. Measuring the phase shift with electron holography

In the present work, the final OAM value was targeted to be $\ell = \pm 1$ as it provides the optimum balance of electron probe size and EMCD signal magnitude [15, 16]. A pure state electron vortex beam is typically of the form:

$$\Psi(r, \theta, z) = A(r) e^{i\ell} e^{ikz} \tag{1}$$

with $\ell \in \mathbb{Z}$ the topological charge of the beam, defining the orbital angular momentum to $l\hbar$, and k the wave vector. For the case $\ell = |1|$, an exact 2π phase shift should arise around the aperture. The Aharonov Bohm phase shift across the needle is sensitive to both electrostatic and magnetic fields via [28]:

$$\Phi(x, y) = C_E \int V(x, y, z) dz - \frac{e}{\hbar} \int A_z(x, y, z) dz \tag{2}$$

where C_E is the interaction constant, $V(x, y, z)$ the three-dimensional electrostatic object potential, e the elementary charge, $\hbar$ the reduced Planck constant, and $A_z(x, y, z)$ the component of the magnetic vector potential parallel to the electron beam propagation direction z. Thus, for our magnetic needle, a 2π phase shift is obtained for a magnetic flux equal to two flux quanta $\Phi_q = \frac{h}{2e}$. In order to optimise the flux in the needles towards the desired two flux quanta, the Aharonov-Bohm phase shift across the needle was measured regularly with conventional electron holography in a TEM while thinning the needles further by FIB until the desired width is obtained. In order to do so, the Qu-An-TEM, an FEI Titan^3 TEM operating at 300 kV in Lorentz mode (objective lens off), was used in a holography setup. A Mllenstedt biprism biased with a 160 V potential allowed interfering two parts of the incoming beam, one passing through vacuum and used as a reference beam, the other part interacting with the region around the tip of the rod. The resulting electron holograms (figures 2.a and 2b) were reconstructed by the Fourier technique with empty holograms used for correcting aberrations coming from the projection and recording systems [29, 30]. Due

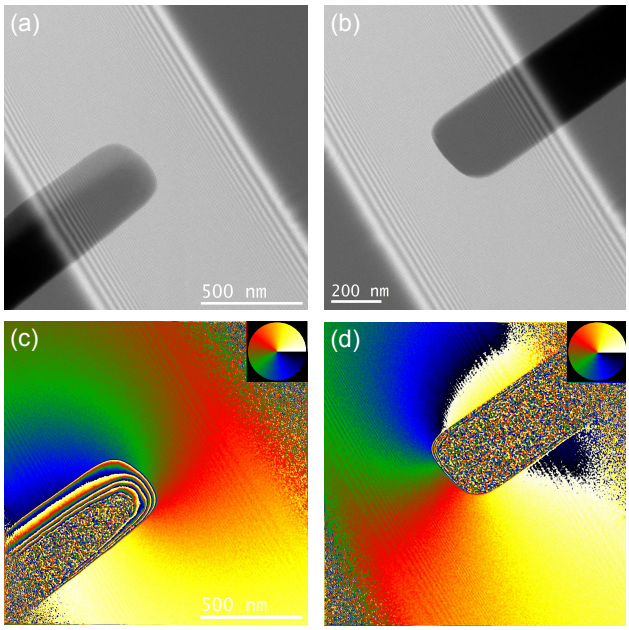

Figure 2: *(a,b) Experimental holograms acquired at the tip of rod ♯1 (a) and rod ♯2 (b). (c,d) Respective phase reconstruction calculated for the experimental holograms. The phase colour map is scaled from 0 to 2π.*

to experimental uncertainty, especially in the positioning of the milling line in the FIB over a 50 μm field of view, the final phase shift values for our two rods were respectively measured as 0.8x2π and 1.2x2π, as displayed in figures 2c and 2d. One could wonder about such a difference in the total phase shift between the two rods knowing they have approximately the same width, but looking at figure 1, a brighter contrast is present on one side of rod ♯1. This contrast likely corresponds to some material redeposition from the FIB, leading to an area which does not contribute to the magnetic field and lowers the total phase shift.

3.2. Confirming the Single magnetic domain state

A prerequisite for the formation of electron vortices with the magnetic monopole-like setup is that the ferromagnetic rod should strictly be made of a single magnetic domain oriented along the long axis of the rod. If this is not the case, flux will escape from the sides of the needle breaking the semi-infinite flux string approximation and leading to unwanted reduced vortex mode purity. In order to verify that only a single magnetic domain is present, a series of holograms were acquired along the length of both rods until reaching the side of the apertures. After careful alignment of the reconstructed holograms and continuous connection of the phase from one image to another, figure 3 is obtained.

One can notice the absence of phase jump along the visible part of the two rods, confirming the single magnetic domain configuration. As expected, the tips of the rods are showing opposite phase ramp handedness, which will lead to electron vortices of opposite OAM sign.

4. Evaluation of vortex mode purity

4.1. Magnetic simulations

The purity of a vortex can be quantitatively evaluated using OAM decomposition of the complete phase profile delimited by the aperture. Unfortunately, it was not experimentally possible to measure the phase distribution over the full 20 μm aperture due to field of view restrictions, and the thick gold protection layer around it preventing a good reference wave to be acquired. However, it is possible to estimate the phase over the entire aperture by using the quantitative measurement obtained at the tip of the rods and extending

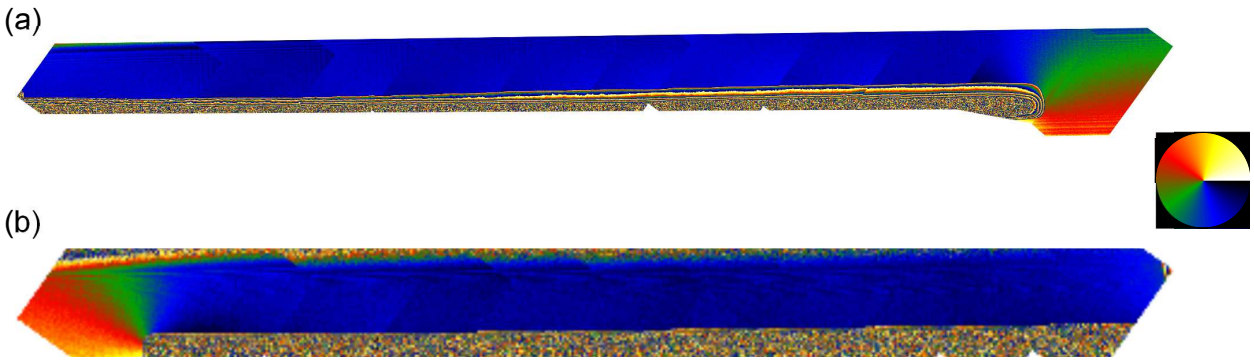

Figure 3: *Reconstructed phase maps issued from holograms series acquired along free standing part of both (a) rod ♯1 and (b) rod ♯2. The phase colour map is scaled from 0 to 2π.*

them via magnetic simulations. To do so, the magnetic rods were approximated by a long cylindrical solenoid carrying a current density $j = I/L$. This hypothesis allows analytical calculation of the magnetic vector potential at every position in space, in the cylindrical coordinates (r, θ, z) [31]:

$$A_\phi = \frac{\mu_0 I}{2\pi}\frac{1}{L}\sqrt{\frac{a}{\rho}}\left[\zeta k\left(\frac{k^2+h^2-h^2k^2}{h^2k^2}K(k^2) - \frac{1}{k^2}E(k^2) + \frac{h^2-1}{h^2}\Pi(h^2,k^2)\right)\right]_{\zeta_-}^{\zeta_+} \tag{3}$$

with μ_0 the magnetic vacuum permeability, I the current in the coils, L the length of the solenoid, a its radius, $\zeta_\pm = z \pm \frac{L}{2}$, $h^2 = \frac{4a\rho}{(a+\rho)^2}$, $k^2 = \frac{4a\rho}{(a+\rho)^2+\zeta^2}$ and $K(k^2)$, $E(k^2)$, $\Pi(h^2,k^2)$ the complete elliptical integrals of the first, second and third kind. The phase map was derived from this equation using numerical integration of the Aharonov-Bohm phase along the beam direction 2. The current I was fitted to match the phase jump at the tip of the rod as observed by electron holography.

4.2. OAM decomposition

The electron wave extrapolated from the calculated phase shift over the full 20 μm aperture can then be decomposed into a basis of pure modes. The analysis was performed following the work of Molina-Terriza et al. and Berkhout et al. by projecting the resulting wave onto a spiral harmonic basis set, $e^{(i\ell\phi)}$, $\ell \in \mathbb{Z}$

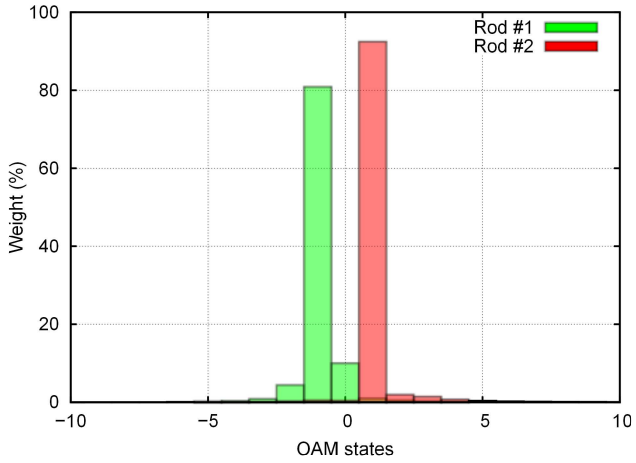

Figure 4: *OAM decomposition of both rods.*

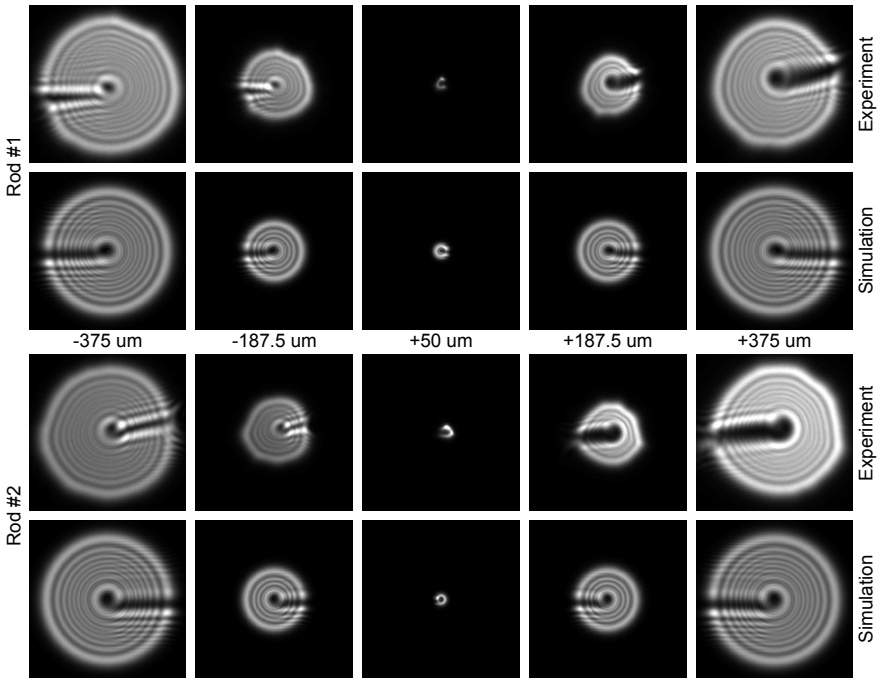

Figure 5: *Far field defocus series for both magnetic rods compared to simulations.*

[32, 33]. In an ideal case, a perfect $\ell = 1$ on axis vortex would give a 100% weight in the $\ell = 1$ state. However, a misalignment of the propagation axis or the presence of other modes will broaden this decomposition. In the present case, both electron waves resulting from the interaction of a plane wave with the two magnetic rods have been calculated and OAM decomposed. The sign of rod ♯1 was arbitrarily chosen to be negative, to be consistent with the handedness of the experimental phase image measured at the tip of the rod. Figure 4 displays the resulting OAM decomposition for rod ♯1 and rod ♯2. Even if both rods are measured to differ approximately 0.2π from the desired total phase shift of 2π, rod ♯2 has a much purer mode distribution, with 92% of the transmitted electrons ending up in the desired $\ell = +1$ state, while only 81% end up in the $\ell = -1$ state for rod ♯1. This difference most likely arises from the non-infinite aspect ratio of our experimental rods. Instead of a perfect radially symmetric phase distribution, expected for a semi-infinite magnetic rod, the equiphase lines centered on the tip of the rods tend to be more bent towards the rods. From the phase simulations, this effect can be partially compensated by slightly increasing the total phase shift across the rod by increasing the flux. With this type of phase profile, the best purity achievable is 98% for a total phase shift across the rod of 1.06x2π, which also explain why rod ♯2 gives a purer OAM.

4.3. Experimental evidence of vortex formation

The above results all seem to confirm the action of the apertures as high purity vortex forming apertures but it is important to have experimental confirmation of the actual presence of vortex beams before further investigations. Two different approaches were considered: *(i)* a through focus series of the far field image and *(ii)* cutting the defocused far field beam by a sharp edge.

The through focus series of the far field images for the two magnetic rods are displayed in figure 5. In both cases, simulations are also added to provide the expected behaviour of the series. One can note the presence of a dark region in the centre of the beam, which never vanishes upon focusing. From a qualitative point of view, the persistence of this dark centre is typical of vortices. Indeed, at the point of the phase discontinuity, the amplitude is forced to remain zero independent of focus. The incomplete azimuthal symmetry when approaching focus is due to the non-integer value of the OAM as well as the presence of

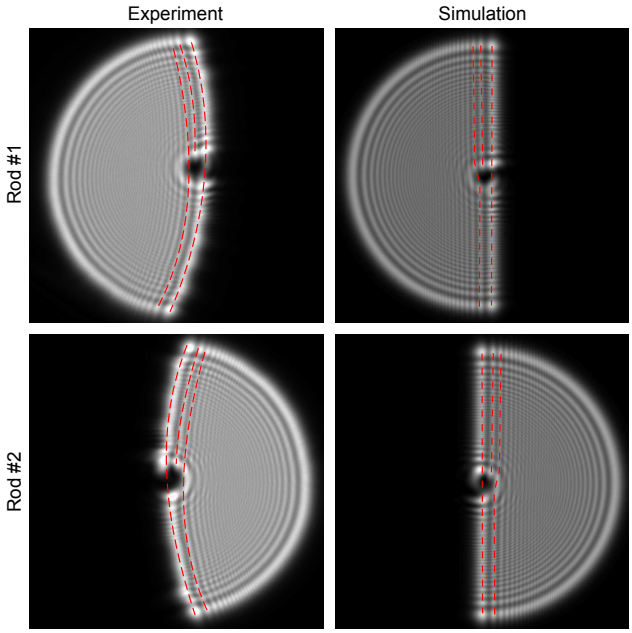

Figure 6: *Sharp edge cutting of the defocused far field image of the rods compared with simulations. On both cases, the extra fringe added upon crossing of the vortex core is clearly visible and is highlighted by the dotted lines.*

the phase reconnection line through the rod. These trends are also reproduced in the numerical simulation via Fourier transforming the complex aperture wave applying the Fresnel defocusing term. There is a slight difference in contrast when comparing over- and under-focused images. This can be attributed to either the presence of a slight defocus of the Lorentz lens in the vortex plane or due to residual electrostatic charging of the aperture.

The existence of a vortex beam can also be revealed by observing Fresnel fringes when imaging a defocused beam that was cut by a sharp edge. Around the vortex centre, a typical fork like pattern should be observed indicating the presence of the vortex core [2]. The appearance of a number of extra fringes at one side directly depends on the average OAM value [34]. In order to perform this experiment, the far field images of the rods were defocused by 1 μm and cut with a 60 μm objective aperture. The experimental images as well as simulated images are displayed in figure 6. An extra fringe is clearly visible for both magnetic rods, revealing their vortex nature, as well as giving a hint about their OAM value, close to ± 1 in the present case.

5. High resolution STEM imaging

In the previous sections we showed that magnetic needle apertures can provide a highly efficient way to create the required spiraling phase shift to produce electron vortex beams of high purity. As the rods themselves cover less than 1% of the aperture area, nearly all the intensity of the incoming beam is converted into a vortex beam. In order to check the ability of such an aperture to create atomic size vortices, the gold coated SiN grid with the two rods was mounted in the condenser plane (C2) of the microscope operating **at 300 kV** in STEM mode, with a semi-convergence angle of 20.6 mrad **and a probe current of 50 pA. The brightness of the electron source was estimated to be 3x10^{1}3 A.m^{-2}.sr^{-1}**. After careful alignment of both probe and image Cs correctors, a high resolution image of SrTiO3 in [001] zone axis was acquired (Figure 7.a). Atomic resolution is nicely visible in the image and both Sr and Ti atomic columns can clearly be identified. The resolution of the image can be estimated to be 87 pm by the presence of all $\langle 420 \rangle$ spots in the FFT (figure 7.b). As a comparison, an equivalent HRSTEM image is displayed in Figure

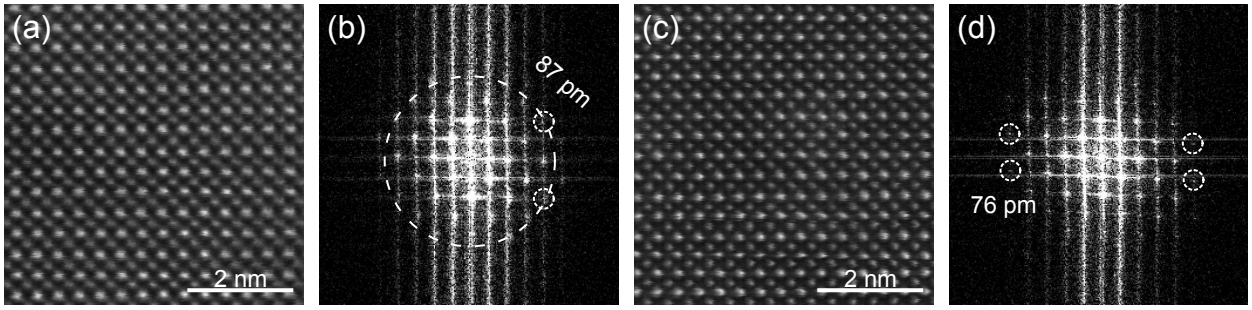

Figure 7: *(a) High resolution STEM image of [001] SrTiO3 using a vortex probe and (b) its corresponding FFT with the (420) spots highlighted. (c) Same image using a standard aperture in the exact same experimental conditions and (d) its corresponding FFT with the (510) spots highlighted.*

7.c, without making use of a vortex probe but rather using a standard 20 μm aperture. In this picture, the $\langle 510 \rangle$ diffraction spots are visible in the FFT, corresponding to a resolution of 76 pm (figure 7.d).

Accordingly, although the atomic columns are slightly broader in the vortex probe images, the resolution between both images is not significantly altered. Moreover, the atomic columns do not present any dark contrast in their centres, as could be expected from the convolution of the vortex probe shape with the atomic columns. The recent work from Löfgren et al. [35] shows from calculations that source size broadening **is mainly responsible of this effect. Indeed, the finite size of the electron source implies that electrons are not all emitted from a single point, and, for a given location of the electron probe, will land on the sample at slightly different positions. This leads to an incoherent addition of shifted pure mode vortices which can be modelled by a convolution with a source intensity profile leading to the disappearing of the dark core. However, It needs to be stressed that this effect will not erase the vortex character as each individual electron still carries OAM and can transfer it, for example during an excitation in the crystal. Depending on the exact interaction that is targeted, this source size broadening effect could or could not lower the visibility of the signal. In order to prove this point, we investigated further a crystal of $Mn_2Sb_2O_7$ aligned in [001] zone axis that was already characterized in a previous study to measure crystal chirality [11]. By lowering the semi-convergence angle to a value of 8.4 mrad, the $\ell = +1$ vortex beam diameter is increased to perfectly match the distance between the three Sb atoms aligned in a triangle shape, a condition which is no longer valid for a standard $\ell = 0$ beam. With these illumination conditions, the ring-like vortex electron beam is no longer smeared out by the source size broadening and the high resolution STEM images reveal the vortex nature of the probe at the atomic scale by a contrast reversal between the $\ell = +1$ and $\ell = 0$ images. Indeed, the contrast reveals bright rings with darker centres on the heavy atomic columns for the $\ell = +1$ beam, as compared to bright spots on the similar columns when a non-vortex aperture is used (Figure 8). This contrast is matching well with multislice simulations reproducing the experimental conditions (Figure 8). This example shows that further improvements in source size brightness would be beneficial for vortex experiments.**

6. Conclusion

We have demonstrated the possibility of creating electron vortex beams using ferromagnetic rods produced from a thin nickel film. The use of a magnetic layer allows to keep the rod width almost perfectly constant over its full length, as required to obtain vortices of high purity. By carefully selecting the width of the magnetic layer by FIB milling, it was possible to obtain electron vortices with average OAM value very close to 1 and more than 90% of the signal ending up in the $|\ell| = 1$ state. This excellent vortex purity competes with values obtained with holographic fork apertures, with the significant advantage of providing

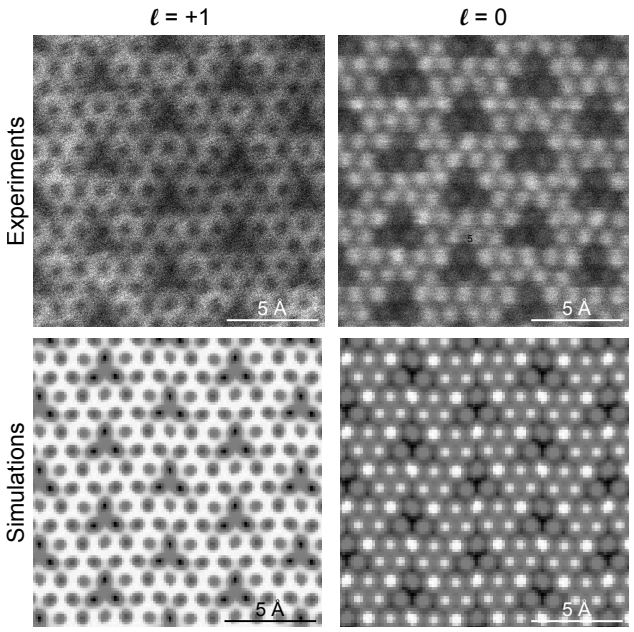

Figure 8: *Experimental high resolution STEM images of a crystal $Mn_2Sb_2O_7$ in [001] zone axis acquired with OAM $\ell = +1$ and $\ell = 0$ electron beams and compared with multislice simulations.*

a single vortex probe of high intensity. As the sizes of the magnetic rods are negligible compared to the aperture, there is almost no loss of electron beam intensity, in contrast to the significant loss resulting from the use of holographic masks. The obtained magnetic rod aperture was then successfully introduced into the condenser plane of a transmission electron microscope to obtain high resolution HAADF STEM images with the use of a vortex probe. An important added benefit of this setup is that the Aharonov-Bohm effect is independent of kinetic energy of the electrons (see Eq. 2). The phase plate then always generates the exact same vortex state, independently of the acceleration voltage. The obtained combination of pure, intense and atomic size vortex beams form an essential step towards the further exploration of atomic resolution EMCD possibly allowing researchers to overcome the severe demands put on the required signal to noise ratio.

7. Acknowledgments

A.B. and J.V. acknowledge funding from the European Research Council under the 7th Framework Program (FP7), ERC Starting Grant No. 278510 VORTEX. J.V. acknowledges funding from FWO project G.0044.13N ('Charge ordering').

8. References

[1] Masaya Uchida and Akira Tonomura. Generation of electron beams carrying orbital angular momentum. *Nature*, 464(7289):737–739, April 2010.

[2] J. Verbeeck, H. Tian, and P. Schattschneider. Production and application of electron vortex beams. *Nature*, 467(7313):301–304, September 2010.

[3] Konstantin Yu. Bliokh, Yury P. Bliokh, Sergey Savelev, and Franco Nori. Semiclassical Dynamics of Electron Wave Packet States with Phase Vortices. *Physical Review Letters*, 99(19):190404, November 2007.

[4] J. F. Nye and M. V. Berry. Dislocations in Wave Trains. *Proceedings of the Royal Society of London A: Mathematical, Physical and Engineering Sciences*, 336(1605):165–190, January 1974.

[5] L. Allen, M. W. Beijersbergen, R. J. C. Spreeuw, and J. P. Woerdman. Orbital angular momentum of light and the transformation of Laguerre-Gaussian laser modes. *Physical Review A*, 45(11):8185–8189, June 1992.

[6] M. W. Beijersbergen, L. Allen, H. E. L. O. van der Veen, and J. P. Woerdman. Astigmatic laser mode converters and transfer of orbital angular momentum. *Optics Communications*, 96(1):123–132, February 1993.
[7] S. M. Lloyd, M. Babiker, J. Yuan, and C. Kerr-Edwards. Electromagnetic Vortex Fields, Spin, and Spin-Orbit Interactions in Electron Vortices. *Physical Review Letters*, 109(25):254801, December 2012.
[8] J. Verbeeck, P. Schattschneider, S. Lazar, M. Stöger-Pollach, S. Löffler, A. Steiger-Thirsfeld, and G. Van Tendeloo. Atomic scale electron vortices for nanoresearch. *Applied Physics Letters*, 99(20):203109, November 2011.
[9] Jo Verbeeck, Giulio Guzzinati, Laura Clark, Roeland Juchtmans, Ruben Van Boxem, He Tian, Armand Béché, Axel Lubk, and Gustaaf Van Tendeloo. Shaping electron beams for the generation of innovative measurements in the (S)TEM. *Comptes Rendus Physique*, 15(23):190–199, February 2014.
[10] Jo Verbeeck, He Tian, and Gustaaf Van Tendeloo. How to Manipulate Nanoparticles with an Electron Beam? *Advanced Materials*, 25(8):1114–1117, February 2013.
[11] Roeland Juchtmans, Armand Béché, Artem Abakumov, Maria Batuk, and Jo Verbeeck. Using electron vortex beams to determine chirality of crystals in transmission electron microscopy. *Physical Review B*, 91(9):094112, March 2015.
[12] Konstantin Y. Bliokh, Peter Schattschneider, Jo Verbeeck, and Franco Nori. Electron Vortex Beams in a Magnetic Field: A New Twist on Landau Levels and Aharonov-Bohm States. *Physical Review X*, 2(4):041011, November 2012.
[13] Igor P. Ivanov and Dmitry V. Karlovets. Detecting Transition Radiation from a Magnetic Moment. *Physical Review Letters*, 110(26):264801, June 2013.
[14] Jérémie Harris, Vincenzo Grillo, Erfan Mafakheri, Gian Carlo Gazzadi, Stefano Frabboni, Robert W. Boyd, and Ebrahim Karimi. Structured quantum waves. *Nature Physics*, 11(8):629–634, August 2015.
[15] P. Schattschneider, S. Rubino, C. Hébert, J. Rusz, J. Kunes, P. Novák, E. Carlino, M. Fabrizioli, G. Panaccione, and G. Rossi. Detection of magnetic circular dichroism using a transmission electron microscope. *Nature*, 441(7092):486–488, May 2006.
[16] Ján Rusz and Somnath Bhowmick. Boundaries for Efficient Use of Electron Vortex Beams to Measure Magnetic Properties. *Physical Review Letters*, 111(10):105504, September 2013.
[17] Ruben Van Boxem, Bart Partoens, and Jo Verbeeck. Inelastic electron-vortex-beam scattering. *Physical Review A*, 91(3):032703, March 2015.
[18] J. Verbeeck, H. Tian, and A. Béché. A new way of producing electron vortex probes for STEM. *Ultramicroscopy*, 113:83–87, February 2012.
[19] Benjamin J. McMorran, Amit Agrawal, Ian M. Anderson, Andrew A. Herzing, Henri J. Lezec, Jabez J. McClelland, and John Unguris. Electron Vortex Beams with High Quanta of Orbital Angular Momentum. *Science*, 331(6014):192–195, January 2011.
[20] Vincenzo Grillo, Gian Carlo Gazzadi, Ebrahim Karimi, Erfan Mafakheri, Robert W. Boyd, and Stefano Frabboni. Highly efficient electron vortex beams generated by nanofabricated phase holograms. *Applied Physics Letters*, 104(4):043109, January 2014.
[21] Tyler R. Harvey, Jordan S. Pierce, Amit K. Agrawal, Peter Ercius, Martin Linck, and Benjamin J. McMorran. Efficient diffractive phase optics for electrons. *New Journal of Physics*, 16(9):093039, 2014.
[22] Ondrej L. Krivanek, Jan Rusz, Juan-Carlos Idrobo, Tracy J. Lovejoy, and Niklas Dellby. Toward Single Mode, Atomic Size Electron Vortex Beams. *Microscopy and Microanalysis*, 20(03):832–836, June 2014.
[23] Roy Shiloh, Yossi Lereah, Yigal Lilach, and Ady Arie. Sculpturing the electron wave function using nanoscale phase masks. *Ultramicroscopy*, 144:26–31, September 2014.
[24] A. Béché, R. Winkler, H. Plank, F. Hofer, and J. Verbeeck. Focused electron beam induced deposition as a tool to create electron vortices. *Micron*, 80:34–38, January 2016.
[25] L. Clark, A. Béché, G. Guzzinati, A. Lubk, M. Mazilu, R. Van Boxem, and J. Verbeeck. Exploiting Lens Aberrations to Create Electron-Vortex Beams. *Physical Review Letters*, 111(6):064801, August 2013.
[26] Ruben Van Boxem, Bart Partoens, and Johan Verbeeck. Rutherford scattering of electron vortices. *Physical Review A*, 89(3):032715, March 2014.
[27] Armand Béché, Ruben Van Boxem, Gustaaf Van Tendeloo, and Jo Verbeeck. Magnetic monopole field exposed by electrons. *Nature Physics*, 10(1):26–29, January 2014.
[28] Y. Aharonov and D. Bohm. Significance of Electromagnetic Potentials in the Quantum Theory. *Physical Review*, 115(3):485–491, August 1959.
[29] Hannes Lichte. Electron holography approaching atomic resolution. *Ultramicroscopy*, 20(3):293–304, 1986.
[30] F. Hüe, C. L. Johnson, S. Lartigue-Korinek, G. Wang, P. R. Buseck, and M. J. Hÿtch. Calibration of projector lens distortions. *Journal of Electron Microscopy*, 54(3):181–190, January 2005.
[31] & Maslen S. H. Callaghan, E. E. The magnetic field of a finite solenoid. *National Aeronautics and Space Administration.*, 465, 1960.
[32] Gabriel Molina-Terriza, Juan P. Torres, and Lluis Torner. Management of the Angular Momentum of Light: Preparation of Photons in Multidimensional Vector States of Angular Momentum. *Physical Review Letters*, 88(1):013601, December 2001.
[33] Gregorius C. G. Berkhout, Martin P. J. Lavery, Miles J. Padgett, and Marco W. Beijersbergen. Measuring orbital angular momentum superpositions of light by mode transformation. *Optics Letters*, 36(10):1863–1865, May 2011.
[34] Andrew G. Peele, Philip J. McMahon, David Paterson, Chanh Q. Tran, Adrian P. Mancuso, Keith A. Nugent, Jason P. Hayes, Erol Harvey, Barry Lai, and Ian McNulty. Observation of an x-ray vortex. *Optics Letters*, 27(20):1752–1754, October 2002.
[35] Vancho Kocevski André Löfgren, Paul Zeiger and Ján Rusz. Influence of nuclear quantum effects on frozen phonon simulations of electron vortex beam haadf-stem images. *Ultramicroscopy*, accepted, January 2016.